

Pattern formation in charge density wave states after a quantum quench

Lingyu Yang, Yang Yang, and Gia-Wei Chern

Department of Physics, University of Virginia, Charlottesville, Virginia 22904, USA

(Received 25 December 2023; revised 23 April 2024; accepted 1 May 2024; published 9 May 2024)

We study postquench dynamics of charge density wave (CDW) order in the square-lattice t - V model. The ground state of this system at half-filling is characterized by a checkerboard modulation of particle density. A generalized self-consistent mean-field method, based on the time-dependent variational principle, is employed to describe the dynamical evolution of the CDW states. Assuming a homogeneous CDW order throughout the quench process, the time-dependent mean-field approach is reduced to the Anderson pseudospin method. Quench simulations based on the Bloch equation for pseudospins produce three canonical behaviors of order-parameter dynamics: phase-locked persistent oscillation, Landau-damped oscillation, and dynamical vanishing of the CDW order. We further develop an efficient real-space von Neumann equation method to incorporate dynamical inhomogeneity into simulations of quantum quenches. Our large-scale simulations uncover complex pattern formations in the postquench CDW states, especially in the strong quench regime. The emergent spatial textures are characterized by super density modulations on top of the short-period checkerboard CDW order. Our demonstration of pattern formation in quenched CDW states, described by a simple broken Z_2 symmetry, underscores the importance of dynamical inhomogeneity in quantum quenches of many-body systems with more complex orders.

DOI: [10.1103/PhysRevB.109.195133](https://doi.org/10.1103/PhysRevB.109.195133)**I. INTRODUCTION**

The postquench dynamics of quantum systems has attracted enormous attention in recent years [1–3]. The interest is partly spurred by tremendous experimental advances both in cold atom systems [4,5] and in ultrafast techniques such as pump-probe spectroscopy [6–11]. In particular, for cold-atomic gases trapped in an optical lattice, the parameters of the Hamiltonian, such as interaction strength between particles and lattice parameters can be tuned rapidly in time, thus providing a near-ideal platform for studying quench-induced nonequilibrium quantum behaviors. Moreover, as cold-atom systems can be well isolated from the environment, their postquench dynamics is well approximated by a unitary evolution. A central question is whether thermalization can be reached in such closed-system quantum evolution and, if yes, what are the mechanisms and timescales [12–24]. Moreover, several nonequilibrium phases and dynamical phase transitions, some of which have no counterpart in equilibrium systems, have been demonstrated in the long-lasting prethermal states after a quantum quench [25–35]. Understanding the nature of such prethermal states is an ongoing active research.

For postquench dynamics with spontaneous symmetry breaking phases, the interplay between the collective modes, as represented by order-parameter fields, and quasiparticle degrees of freedom dominates the nonequilibrium behaviors of the prethermal states [36,37]. Extensive theoretical studies, including several pioneering works on the interaction quench of superconductor pairing field, have revealed three dynamical phases of the time-dependent order parameter in the collisionless limit [38–42]. In the phase-locked regime, the dynamics of the collective modes locks with that of the quasiparticles, giving rise to a persistent oscillation of the order parameter.

For intermediate quench amplitudes, the perturbed system relaxes to a state with a reduced order parameter through the Landau-damping mechanism. The energy transfer from the collective modes to quasiparticles in this regime leads to a damped oscillation of the order parameter. Finally, in the third strongly damped regime, corresponding to a quench toward reduced interactions, the relaxation of the system is characterized by dynamically vanishing order parameters. While more complex dynamical behaviors have also been discussed, most symmetry-breaking phases, including the well-studied BCS superconductivity (SC) and spin density waves (SDW) as well as more complex order parameters, exhibit the above three major dynamical regimes [43–56].

It is worth noting that in most previous studies the prethermal states induced by interaction quenches are assumed to be spatially homogeneous, including the three main dynamical phases discussed above. For example, the Anderson pseudospin approach [57], which is widely used in the study of quench dynamics of BCS superconductors, precludes the possibility of spatial fluctuation or inhomogeneity. On the other hand, since thermalization mechanisms are generally local, it is likely that the postquench states would develop spatial inhomogeneity through a process similar to the Kibble-Zurek mechanism [58,59]. For the case of interaction quench, significant amount of energy is uniformly injected into a system. The relaxation of local regions that are separated from each other by a distance greater than the coherent length would proceed independently. Such incoherent local relaxations lead to the generation of topological defects of the order parameter, giving rise to a heterogeneous postquench state [60–65].

Even in the collisionless coherent regime, the highly nonlinear postquench evolution renders the system susceptible to instabilities that could lead to inhomogeneous

states. For example, it is shown that quench-induced large-amplitude coherent oscillations of the SC order parameter are unstable against parametric instability and the emergence of Cooper-pair turbulence [66]. Spontaneous formation of inhomogeneous superconducting states following an interaction quench has indeed been demonstrated in real-space dynamical simulations based on time-dependent Hartree-Fock-Bogoliubov theory [67,68]. Similar scenario has also been observed in the context of Mott transitions in Hubbard models. Although the Mott metal-insulator transition is not characterized by the broken-symmetry scenario, the on-site double occupation probability serves as an effective order parameter of a Mott transition. Interestingly, the double-occupancy of a quenched Hubbard model exhibits a coherent oscillation similar to that of conventional order parameters [69,70]. Real-space dynamical simulations of Mott phases in the coherent collisionless limit also found postquench states with a highly inhomogeneous distribution of the double occupancy [71].

While dynamical inhomogeneity in quantum quenches of many-body systems remains to be systematically investigated, pattern formation phenomena are ubiquitous in nonequilibrium systems with highly nonlinear dynamics. In particular, the mechanisms and characterizations of pattern formation in classical physics, soft-matter, and biological systems have been intensively studied for decades [72–76]. Several unifying descriptions of pattern forming systems, such as the Swift-Hohenberg equation, as well as classifications of universal behaviors have also been developed. It remains to be seen whether some of the general mathematical frameworks can be applied to pattern formation induced by quantum quenches. However, the physical mechanisms of pattern-forming instabilities in quantum quenches are intrinsically different. For most classical examples, the formation of complex patterns often is driven by energy injection and the subsequent local dissipation in an open system. On the other hand, the complex textures of order-parameter field in postquench states result from the unitary evolution of a closed quantum system.

In this paper, we demonstrate quench-induced pattern formations in a system with a broken Z_2 symmetry, which is perhaps one of the simplest symmetry-breaking phases, of a fermionic system. Specifically, we present extensive simulations on the interaction quench of the square-lattice t - V model, which exhibits a checkerboard charge density wave (CDW) order at half-filling. As the checkerboard charge modulation breaks the sublattice symmetry of the square lattice, the resultant CDW order is characterized by a Z_2 Ising order parameter. A time-dependent mean-field approach is employed to describe the coherent dynamics of the perturbed t - V model. Assuming homogeneous CDW order throughout the quench process, the coherent dynamics of the postquench CDW states can be modeled by an Anderson pseudospin theory, similar to the ones used for quench dynamics of BCS superconductors. To incorporate dynamical inhomogeneities into the quench simulations, we further develop a real-space nonlinear von Neumann equation formulation that allows for efficient large-scale simulations.

The main results of our extensive quench simulations are summarized in a phase diagram of dynamical regimes shown in Fig. 1. Simulation results based on pseudospin methods

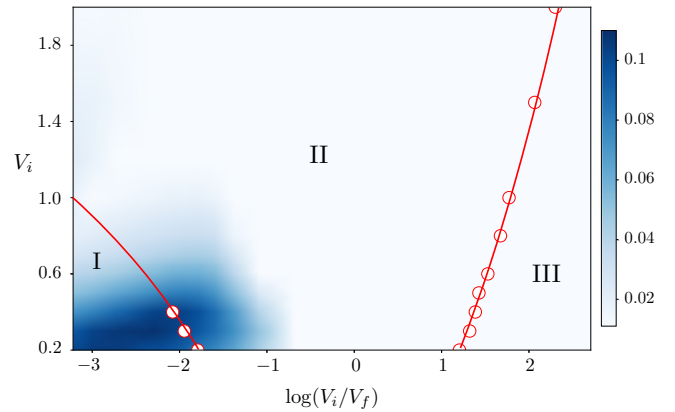


FIG. 1. Phase diagram of postquench CDW states of the square-lattice t - V model. V_i and V_f denote the density-density repulsion before and after the sudden quench. The three dynamical phases are: (I) phase-locked persistent oscillation, (II) Landau-damped oscillation, (III) overdamped oscillation with a vanishing CDW order. The data points are obtained from the Anderson pseudospin method based on the assumption that a homogeneous CDW order persists in the postquench states. Large-scale quench simulations based on the real-space von Neumann equation are used to study quench-induced dynamical inhomogeneity. The color intensity indicates the spatial inhomogeneity of density modulation in the postquench states.

show that the postquench CDW order exhibits the three canonical dynamical phases discussed above: (I) phase-locked persistent oscillation, (II) Landau-damped oscillation with a finite asymptotic value, and (III) dynamical vanishing of the CDW order parameter. Remarkably, our real-space simulations uncover inhomogeneous CDW states with complex modulation patterns in both the phase-locked and Landau-damping regimes, suggesting an important dynamical phase characterized by pattern formation in the postquench states. Further characterizations of these dynamical phases will be discussed in the following sections.

It should be noted that the above postquench dynamical behaviors are obtained based on time-dependent Hartree-Fock method. While such mean-field approaches could give exact solutions for models with infinite-range interactions, they are known to apply only to the short and intermediate time regimes and break down at late times for systems with short-range interactions [77]. This is consistent with the fact that such short-range systems, including the t - V model considered in this paper, typically thermalize at late times after quench, especially when quasiparticle relaxations set in. In particular, this also means that persistent oscillations in the phase-locked regime will eventually decay at timescale larger than the quasiparticle relaxation times.

The rest of the paper is organized as follows. In Sec. II, we briefly review the theory of time-dependent Hartree-Fock (TDHF) theory from the viewpoint of Dirac-Frenkel variational principle and demonstrate the approach on the t - V model. In Sec. III, an Anderson pseudospin formulation for the quench dynamics of CDW is derived from the general theory under the assumption of a homogeneous CDW order. We then reformulate the general real-space TDHF method as a nonlinear von Neumann equation for the single-fermion density matrix in Sec. IV. The characterizations of the

dynamical inhomogeneity are discussed and analyzed in detail in Sec. V. Finally, we conclude the paper with a summary and outlook in Sec. VI.

II. TIME-DEPENDENT HARTREE-FOCK METHOD FOR THE t - V MODEL

We consider the quantum quench dynamics of the spinless fermionic t - V model on a square lattice. This model, which can be viewed as a simplified version of the Hubbard model, describes the competition between delocalization of fermions on a lattice and the nearest-neighbor density-density repulsion. Its Hamiltonian reads

$$\hat{\mathcal{H}} = -t_{\text{nn}} \sum_{\langle ij \rangle} \hat{c}_i^\dagger \hat{c}_j + V \sum_{\langle ij \rangle} \hat{n}_i \hat{n}_j, \quad (1)$$

where \hat{c}_i^\dagger (\hat{c}_i) denotes the creation (annihilation) operator of a spinless fermion at site i , $\hat{n}_i = \hat{c}_i^\dagger \hat{c}_i$ is the fermion number operator. The first term above describes particle hopping between neighboring sites $\langle ij \rangle$ on a square lattice, with t_{nn} being the transfer coefficient. The second term with $V > 0$ represents a nearest-neighbor density-density repulsive interaction.

For a half-filled t - V model defined on a bipartite lattice, the ground state in the strong coupling limit $V \rightarrow \infty$ is obtained when one sublattice is fully occupied, while the other sublattice is empty. This staggered arrangement of fermions breaks the Z_2 sublattice symmetry and can be described by an Ising order parameter. For the case that the fermionic particles are electrons, the resultant density modulation corresponds to a charge density wave (CDW) order. Although the t - V model is also often used to describe charge-neutral fermionic cold atoms, we shall refer to a periodic particle-density modulation as a CDW for convenience. In the case of a square-lattice, a divergent Lindhard susceptibility due to a perfect Fermi surface nesting at half-filling indicates that the system is unstable against the formation of a checkerboard CDW order even in the small V limit.

For a finite repulsive interaction, the t - V model cannot be exactly solved either for equilibrium states or dynamical evolution. The 1D version of this model can be efficiently solved with high accuracy using the density matrix renormalization group (DMRG) [78,79] and its time-dependent generalizations such as time-evolving block decimation (TEBD) algorithm [80,81]. Indeed, the infinite-system TEBD methods have been applied to simulate the interaction quench of the 1D t - V model, which is equivalent to an spin-1/2 XXZ chain [82,83]. In particular, for an initial state with a classical Néel order (corresponding to $V \rightarrow \infty$ limit), a sudden quench to a finite V leads to the melting of the CDW order, which is characterized by broad probability distribution of local CDW order [83]. Although DMRG or tensor-network variational wave functions can also be applied to quasi-2D systems, e.g., with a cylinder geometry, such approaches are computationally more intensive with less well-controlled accuracy. Large-scale dynamical simulations of higher-dimensional systems are thus not feasible using such DMRG-based methods.

The Hartree-Fock (HF) mean-field method proves an efficient approximation to the modeling of the emergent CDW states. The central idea of HF approximation, as in most mean-field type methods, is to reduce a many-body problem into

an effective single-particle problem self-consistently. While such self-consistency can be achieved via the usual mean-field decoupling of the interaction terms, HF approximation is best understood as a variational method in which the trial many-fermion wave function has the form of a Slater determinant. The HF or its extension for superconducting pairing have also been generalized to include time dependence. Indeed, the time-dependent HF (TDHF) is widely used to describe dynamics of many-body systems in nuclear physics and quantum chemistry [84–86]. It is worth noting that the Anderson pseudospin approaches [38–42] to quantum quenches of SC or SDW orders are also based on TDHF.

Generalization of the mean-field methods to dynamical evolution of interacting systems can be achieved via the Dirac-Frenkel time-dependent variational principle (TDVP) [87,88]. By constraining a quantum state to a specific manifold of the Hilbert space through a variational wave function, the minimum action equation gives an effective dynamical description for the variational parameters. For example, applying TDVP to variational matrix product states (MPS) offers an alternative approach to introduce time evolution in DRMG-based methods [89,90]. The TDHF methods, or more generally the time-dependent self-consistent field methods for fermions, can similarly be derived by constraining the many-body wave function to the form of Slater determinant in the TDVP formalism. Here we outline the approach for a generalized t - V model with both particle hopping t_{ij} and density-density interaction V_{ij} extended to further neighbor pairs (ij) . The derivation can be straightforwardly generalized to other lattice models.

We start with the Dirac-Frenkel action for a general quantum state $|\Psi(t)\rangle$ whose dynamics is governed by a Hamiltonian $\hat{\mathcal{H}}$,

$$S[\Psi] = \int dt \langle \Psi(t) | \left(i\hbar \frac{d}{dt} - \hat{\mathcal{H}} \right) | \Psi(t) \rangle. \quad (2)$$

The equation of motion for the quantum state is given by the least action principle, $\partial S / \partial \langle \Psi | = 0$. Indeed, the minimum action equation simply reproduces the Schrödinger equation for an unconstrained wave function. Next we assume that the many-fermion quantum state is a Slater determinant, which can be expressed as a filled Fermi sea of self-consistently determined quasiparticles,

$$|\Psi(t)\rangle = \prod_{\mu} \hat{\gamma}_{\mu}^{\dagger}(t) |0\rangle, \quad (3)$$

where $\hat{\gamma}_{\mu}^{\dagger}(t)$ is the time-dependent creation operator of a quasiparticle with quantum number μ and $|0\rangle$ is the vacuum of the fermions. The quasiparticle operators are related to the fermion operators \hat{c}_i^{\dagger} through a time-dependent unitary transformation,

$$\hat{\gamma}_{\mu}^{\dagger}(t) = \sum_i \phi_i^{\mu}(t) \hat{c}_i^{\dagger}. \quad (4)$$

As will be shown below, the transformation coefficients ϕ_i^{μ} play the role of effective single-particle wave functions. The independence of the quasiparticles further imposes the orthogonality conditions for the wave functions $\sum_i \phi_i^{\mu*}(t) \phi_i^{\nu}(t) = \delta_{\mu\nu}$, which have to be satisfied at all times. Substituting the

Slater determinant wave function into the Dirac-Frenkel action and using the Wick's theorem to compute the expectation values, we obtain

$$S[\{\phi\}] = \int dt \sum_{\mu} \sum_{ij} \left[\phi_i^{\mu*} \left(i\hbar \delta_{ij} \frac{d}{dt} + t_{ij} \right) \phi_j^{\mu} \right] - \int dt \sum_{\mu, \nu} \sum_{ij} V_{ij} (|\phi_i^{\mu}|^2 |\phi_j^{\nu}|^2 - \phi_i^{\mu*} \phi_j^{\nu*} \phi_j^{\mu} \phi_i^{\nu}). \quad (5)$$

The two terms in the second line above correspond to the familiar Hartree and Fock decoupling, respectively. The least action condition $\partial S / \partial \phi^{\mu*} = 0$ gives the following nonlinear single-particle Schrödinger equations:

$$i\hbar \frac{d\phi_i^{\mu}}{dt} = - \sum_j t_{ij} \phi_j^{\mu} + \sum_j \sum_{\nu} V_{ij} |\phi_j^{\nu}|^2 \phi_i^{\mu} - \sum_j \sum_{\nu} V_{ij} \phi_j^{\nu*} \phi_i^{\nu} \phi_j^{\mu}. \quad (6)$$

The coupled differential equations of these single-particle wave functions give a complete dynamical description of the many-fermion systems. Importantly, for a given set of initial wave functions $\phi_i^{\mu}(t=0)$ that are normalized and orthogonal to each other, it can be shown that the orthogonality conditions are maintained by the above dynamical equations.

III. ANDERSON PSEUDOSPIN FORMULATION

Here we derive an effective spin formulation for the coherent dynamics of CDW from the general TDHF equations. For a bipartite lattice, the nearest-neighbor repulsive density-density interaction naturally leads to a disparity of particles on the two sublattices. The resultant long-range order corresponds to a commensurate CDW state with an ultrashort modulation period. In the case of square lattice, this CDW order is characterized by a checkerboard pattern associated with the wave vector $\mathbf{Q} = (\pi, \pi)$. For a time-dependent CDW state, an effective order parameter for the charge modulation is

$$\Delta(t) = \frac{1}{N} \sum_i \langle \Psi(t) | \hat{n}_i | \Psi(t) \rangle e^{i\mathbf{Q} \cdot \mathbf{r}_i}, \quad (7)$$

where $\hat{n}_i = \hat{c}_i^{\dagger} \hat{c}_i$ is the number operator of fermions at site i , and the phase factor $\exp(i\mathbf{Q} \cdot \mathbf{r}_i) = \pm 1$ for the two sublattices. Within the TDHF framework, the time-dependent many-fermion state $|\Psi(t)\rangle$ is to be approximated by the Slater determinant state in Eq. (3). Assuming that the postquench system remains in a homogeneous CDW state, which means the $\mathbf{Q} = (\pi, \pi)$ checkerboard pattern is the only Fourier mode of the particle fluctuations, there are only two different values of the on-site particle number depending on the sublattices,

$$n_{A/B}(t) = \bar{n} \pm \Delta(t). \quad (8)$$

Here $\bar{n} = 1/2$ is the average number of particles per site. Importantly, the assumption that the time-evolving postquench system preserves a homogeneous CDW order indicates an emergent translation symmetry associated with the checkerboard pattern, which is a 45° -rotated square lattice with a

doubled unit cell. This in turn implies that wave vectors \mathbf{k} , restricted to the reduced Brillouin zone, are good quantum numbers of the time-dependent CDW states. We thus introduce the following ansatz for the wave functions of quasiparticles:

$$\phi_i^{\mathbf{k}}(t) = \frac{e^{i\mathbf{k} \cdot \mathbf{r}_i}}{\sqrt{N}} \eta_{\mathbf{k}}^{s_i}(t), \quad (9)$$

where $s_i = A, B$ denotes the sublattice of site i . The time evolution of $\eta_{\mathbf{k}}^s(t)$ is governed by the Fourier transform of the time-dependent Schrödinger equation (6),

$$i\hbar \frac{d}{dt} \begin{pmatrix} \eta_{\mathbf{k}}^A \\ \eta_{\mathbf{k}}^B \end{pmatrix} = \begin{pmatrix} -V \Delta(t) & \epsilon_{\mathbf{k}} \\ \epsilon_{\mathbf{k}} & +V \Delta(t) \end{pmatrix} \begin{pmatrix} \eta_{\mathbf{k}}^A \\ \eta_{\mathbf{k}}^B \end{pmatrix}, \quad (10)$$

where $\epsilon_{\mathbf{k}} = -2t_{\text{nn}}(\cos k_x + \cos k_y)$ is the dispersion relation of square-lattice tight-binding model. Since the CDW order is driven by the Hartree term, we have neglected the Fock exchange term for simplicity. We have also dropped the constant diagonal term $V\bar{n}$, which contributes only to an overall phase of the wave functions. Using the ansatz (9) for the Slater determinant in Eq. (7), the time-dependent CDW order parameter is given by

$$\Delta(t) = \sum_{\mathbf{k}} (|\eta_{\mathbf{k}}^A(t)|^2 - |\eta_{\mathbf{k}}^B(t)|^2). \quad (11)$$

The dynamical equation of the CDW state is then reduced to that of a collection of two-level systems, each associated with a wave vector \mathbf{k} . An intuitive description of a dynamical two-level system is given by the Anderson pseudospin approach [57]. To this end, we introduce an effective spin $\mathbf{S}_{\mathbf{k}}$ for each wave vector \mathbf{k} , with the following definition:

$$\begin{aligned} S_{\mathbf{k}}^x &= \eta_{\mathbf{k}}^{A*} \eta_{\mathbf{k}}^B + \eta_{\mathbf{k}}^{B*} \eta_{\mathbf{k}}^A, \\ S_{\mathbf{k}}^y &= -i(\eta_{\mathbf{k}}^{A*} \eta_{\mathbf{k}}^B - \eta_{\mathbf{k}}^{B*} \eta_{\mathbf{k}}^A), \\ S_{\mathbf{k}}^z &= |\eta_{\mathbf{k}}^A(t)|^2 - |\eta_{\mathbf{k}}^B(t)|^2. \end{aligned} \quad (12)$$

Since the A and B sublattices are related by the wave vector $\mathbf{Q} = (\pi, \pi)$, as will be shown in the next section, each pseudospin $\mathbf{S}_{\mathbf{k}}$ thus represents the dynamical degree of freedom for a fundamental particle-hole pair with momenta \mathbf{k} and $\mathbf{k} + \mathbf{Q}$. The dynamics of these effective spins is governed by the Bloch equation [91],

$$\frac{d\mathbf{S}_{\mathbf{k}}}{dt} = \mathbf{B}_{\mathbf{k}}(t) \times \mathbf{S}_{\mathbf{k}}, \quad (13)$$

which essentially describes the Landau-Lifshitz precession dynamics with a time-dependent magnetic field

$$\mathbf{B}_{\mathbf{k}}(t) = \frac{2}{\hbar} (\epsilon_{\mathbf{k}}, 0, -V \Delta(t)). \quad (14)$$

Note that the Bloch equations for different spins are coupled to each other through the z component of the magnetic field. From the definition Eq. (11), we have $B^z(t) = -V \sum_{\mathbf{k}} S_{\mathbf{k}}^z(t)$, which shows that the magnetic field that drives the spin dynamics originates from individual pseudospins.

In the following, we apply the above coupled Bloch equations to simulate the interaction quench of the CDW order of the t - V model at half-filling. As discussed in Sec. II, due to a perfect nesting of the Fermi surface at half-filling, the system is unstable against the formation of checkerboard CDW order

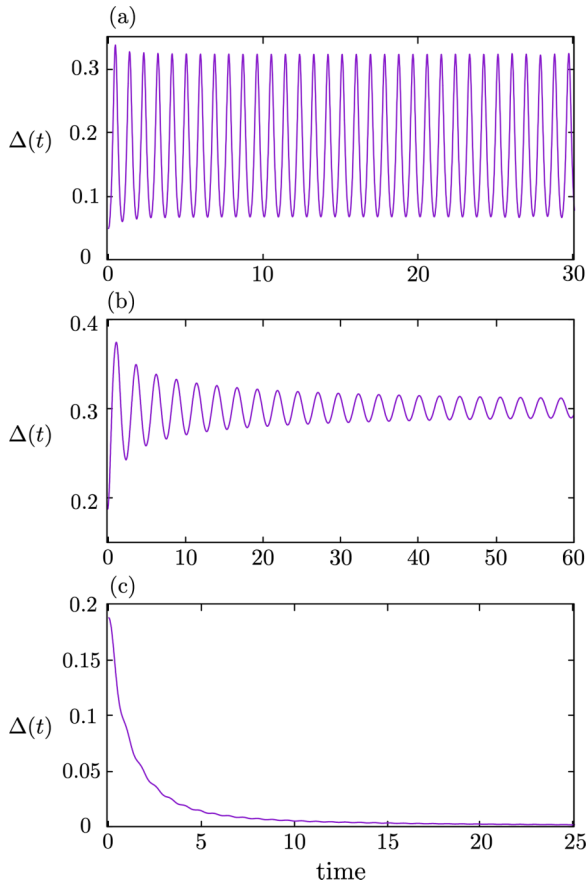


FIG. 2. The time dependence of the CDW order parameter $\Delta(t)$ obtained from the pseudospin simulations. The three panels show the three main dynamical regimes of a quantum quench: (a) phase-locked regime with persistent oscillation ($V_i = 0.2$, $V_f = 5.0$), (b) Landau-damping regime ($V_i = 0.5$, $V_f = 1.0$), and (c) overdamped regime with a dynamical vanishing of the order parameter ($V_i = 0.5$, $V_f = 0.1$).

for an arbitrarily small V . In our interaction quench simulations, the system is initially prepared in the mean-field ground state of the t - V model with the interaction fixed at an initial value V_i . At time $t = 0$, the interaction is suddenly changed to V_f . The quantum quench simulation can also be viewed as the time evolution of a system, which is initialized in a CDW state stabilized by V_i at $t = 0$ and is subject to an time-independent Hamiltonian with V_f for $t > 0$.

Our simulations summarized in Fig. 2 show that the postquench CDW order exhibits the three major dynamical behaviors common to order parameters of other symmetry-breaking phases discussed in Sec. I. First, in the phase-locked regime corresponding to a strong quench with $V_f/V_i \gg 1$, the CDW order parameter exhibits a persistent oscillation after a short transient period, as shown in Fig. 2(a). In this regime, the precessional dynamics of individual pseudospins synchronizes with one another to produce an oscillating B field that drives their own oscillatory dynamics self-consistently. Physically, this describes a synchronized oscillation of the collective CDW order parameter and individual particle-hole pairs.

For intermediate quenches such that the static CDW order parameters before and after the quench are similar $\Delta_f \sim \Delta_i$, the sudden change of interaction again results in an oscillation of the CDW order parameter. Yet, the amplitude of the oscillation decreases with time and the CDW order gradually settles to a different value at large time; see Fig. 2(b). More specifically, the decay of the oscillation amplitude follows a $1/\sqrt{t}$ power law, as in the interaction quench of BCS superconductor and SDW. This dynamical behavior is similar to the Landau-damping phenomena in plasma physics and numerous other physical systems. The decaying oscillation of the order parameter results from a dissipationless energy transfer from the collective modes to quasiparticle excitations [39,92]. This damping can also be understood as a result of the increasingly incoherent precessional motions of pseudospins, which fail to produce a self-sustaining driving force.

Finally, for quenches toward to a much smaller interaction, $V_f \ll V_i$, the postquench state exhibits a dynamical vanishing of the CDW order as shown in Fig. 2(c). In this regime, the magnetic field in Eq. (14) is dominated by the kinetic energy term. As the precession dynamics of individual particle-hole pairs resorts to their respective natural frequencies, the resultant dephasing leads to an overdamping of the CDW order. It is worth noting that here the quenched system relaxes to a state with a vanishing CDW, despite the fact that a finite CDW order is expected to exist for a nonzero $V_f > 0$ due to the Fermi-surface nesting instability discussed above. Although the system cannot really thermalize under the TDHF evolution, the vanishing CDW order can be intuitively understood as a result of the system being in a quasi-equilibrium state of a temperature that is higher than the critical T_c of V_f . Inclusion of dissipative mechanisms in the postquench evolution is thus expected to bring the CDW order back to the static Δ_f .

We also note that, instead of an exponential decay as in the case of quench dynamics of BCS pairing, the decline of the CDW order, which sometimes is accompanied by a small oscillation, follows a $1/t$ power law, similar to the case of SDW order in the quantum quench of square lattice Hubbard model [49]. This algebraic decay could be attributed to the nonanalyticity of the density of states of the square-lattice tight-binding model at half-filling [49].

IV. REAL-SPACE VON NEUMANN EQUATION

The Anderson pseudospin approaches discussed in the previous section are widely used in the study of quantum quenches of various symmetry-breaking phases including superconductivity and spin-density waves. As the pseudospin methods assume the persistence of a perfect long-range order after the quench, these previous studies thus preclude any spatial inhomogeneity in the postquench states. To go beyond the pseudospin methods and allow for spatial fluctuations after a quantum quench, here we discuss an efficient real-space formulation of TDHF in terms of correlation function $\rho_{ij} = \langle \hat{c}_j^\dagger \hat{c}_i \rangle$, also known as the single-particle density matrix. From the definition of the Slater determinant in Eqs. (3) and (4), the density matrix is related to the time-dependent single-particle

wave functions as

$$\rho_{ij}(t) = \langle \Psi(t) | c_j^\dagger c_i | \Psi(t) \rangle = \sum_{\mu} \phi_i^{\mu}(t) \phi_j^{\mu*}(t). \quad (15)$$

Compared with time-dependent Schrödinger equation (6) for the effective wave functions, the density matrix approach has the advantage that ρ_{ij} is directly related to observables and the corresponding equation of motion is amenable to efficient numerical simulations.

The pseudospins $\mathbf{S}_{\mathbf{k}}$ in Sec. III actually correspond to the Fourier transform of the density matrix elements, which are given by

$$\rho_{\mathbf{q},\mathbf{q}} = \langle \hat{c}_{\mathbf{q}}^\dagger \hat{c}_{\mathbf{q}} \rangle, \quad (16)$$

where $\hat{c}_{\mathbf{q}} = (1/\sqrt{N}) \sum_i \hat{c}_i e^{-i\mathbf{q}\cdot\mathbf{r}_i}$ denotes the fermion operator in momentum space. In the presence of a perfect CDW order, the only nonzero matrix elements are $\rho_{\mathbf{k},\mathbf{k}}$ and $\rho_{\mathbf{k},\mathbf{k}+\mathbf{Q}}$, where wave vectors \mathbf{k} are now restricted to the reduced Brillouin zone. The effective spins are then given by

$$\begin{aligned} S_{\mathbf{k}}^x &= \frac{1}{2}(\rho_{\mathbf{k},\mathbf{k}} - \rho_{\mathbf{k}+\mathbf{Q},\mathbf{k}+\mathbf{Q}}), \\ S_{\mathbf{k}}^y &= -\text{Im} \rho_{\mathbf{k},\mathbf{k}+\mathbf{Q}}, \quad S_{\mathbf{k}}^z = \text{Re} \rho_{\mathbf{k},\mathbf{k}+\mathbf{Q}}. \end{aligned} \quad (17)$$

This simple analysis further highlights the fact that the pseudospin approach precludes inhomogeneous postquench states. The onset of spatial fluctuations thus corresponds to the emergence of nonzero matrix elements $\rho_{\mathbf{k},\mathbf{k}+\mathbf{q}}$ with incommensurate wave vectors $\mathbf{q} \neq \mathbf{Q}$.

The dynamical equation that governs the time dependence of ρ_{ij} can be directly obtained from the time-dependent Schrödinger equation (6). An alternative, which is physically more intuitive, is to use the “first-quantized” formulation of the mean-field Hamiltonian. To this end, we note that from the standard mean-field decoupling for the interaction term, $\hat{n}_i \hat{n}_j \rightarrow \langle \hat{n}_i \rangle \hat{n}_j + \hat{n}_i \langle \hat{n}_j \rangle = \rho_{ii} \hat{n}_j + \rho_{jj} \hat{n}_i$, one can define a time-dependent mean-field Hamiltonian

$$\hat{\mathcal{H}}_{\text{MF}}(t) = \sum_{ij} \hat{c}_i^\dagger H_{ij}[\rho(t)] \hat{c}_j, \quad (18)$$

where the first-quantized Hamiltonian has a simple form

$$H_{ij} = -t_{ij} + \delta_{ij} v_i(t). \quad (19)$$

The first term represents the kinetic energy, and the second term denotes an effective on-site potential

$$v_i(t) = V \sum_j' \rho_{jj}(t), \quad (20)$$

where \sum_j' indicates summation over sites j that are nearest neighbors to i . This Hamiltonian can also be read directly from the form of the time-dependent Schrödinger equation in (6). The single-particle density matrix then satisfies a self-consistent nonlinear von Neumann equation,

$$-i\hbar \frac{d\rho}{dt} = [\rho, H(\rho)], \quad (21)$$

where ρ and H denote the $N \times N$ matrix of the density matrix and the first-quantized Hamiltonian, respectively. Using Eq. (19), the explicit von Neumann equation for the density

matrix is

$$-i\hbar \frac{d\rho_{ij}}{dt} = (v_j - v_i)\rho_{ij} + \sum_k (t_{ik}\rho_{kj} - \rho_{ik}t_{kj}). \quad (22)$$

The CDW order parameter in Eq. (7) can be straightforwardly computed from the diagonal matrix elements

$$\Delta(t) = \frac{1}{N} \sum_i \rho_{ii}(t) e^{i\mathbf{Q}\cdot\mathbf{r}_i}. \quad (23)$$

It is worth noting that for a system of N sites, there are $N/2$ pseudospins, each indexed by a wave vector \mathbf{k} in the reduced Brillouin zone. The computational complexity of solving the coupled Bloch equations is thus of order $O(N)$. On the other hand, the number of independent matrix elements of ρ scales as N^2 for general Slater determinant states with potential spatial inhomogeneity. Integration of the von Neumann equation using a naive matrix-matrix multiplication method would lead to a $O(N^3)$ complexity. The von Neumann equation formulation allows one to take advantage of efficient sparse matrix multiplication algorithms, thus improving the computational efficiency. It is worth noting that even though the TDHF approach essentially reduces the many-body problem to an effective single-particle one, additional complexity is required for evolving a density matrix or equivalently a Slater determinant in order to account for the quantum statistics of identical fermions.

Applying the von Neumann equation method to simulate quantum quenches of the t - V model up to $N = 70 \times 70$ systems, we first confirm that, for the same system sizes, the real-space approach exactly reproduces the Landau-damped and overdamped oscillations when the V_i, V_f parameters are set to those used in Fig. 2. Yet, for most of the strong quench regime where phase-locked oscillation is expected, our large-scale simulations observe a CDW dynamics that is distinctly different from the three dynamical regimes discussed above; two such examples are shown in Fig. 3. In both cases, the interaction is quenched from a small V_i to a much larger V_f . As discussed in Sec. II, the pseudospin simulations for such strong quench regime predicts a persistent oscillation of the CDW order parameter in the postquench states. Instead, the CDW time traces shown in Fig. 3 exhibit damped oscillations and a finite asymptotic value, similar to the Landau-damping behavior.

However, contrary to the algebraic $1/\sqrt{t}$ decay characteristic of the Landau-damping regime, here we observe a much faster decay of the oscillation amplitudes. In fact, the decline of the oscillation is even accelerated before the CDW order eventually collapses to a nearly constant value. This seemingly complex dynamical behaviors in time domain are not caused by a complex order parameter as in some previous studies. Instead, as we show in the next section, the collapsed oscillation of the CDW order is due to the emergence of inhomogeneous postquench states.

V. DYNAMICAL INHOMOGENEITY AND PATTERN FORMATION

The CDW order parameter $\Delta(t)$ computed in Eq. (23) only represents the overall difference of particles in the two

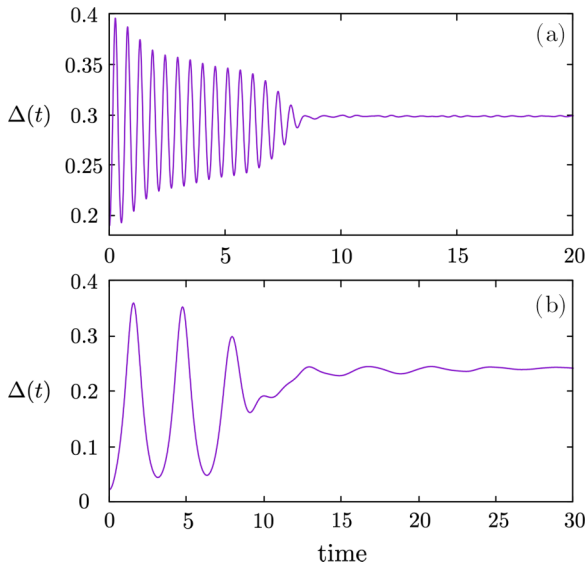


FIG. 3. The overall CDW order parameter $\Delta(t)$ as a function of time in the regime of spatially inhomogeneous postquench states. The quench parameters are: (a) $V_i = 0.5$ to $V_f = 5.0$, and (b) $V_i = 0.1$ to $V_f = 1.5$. Snapshots of the emergent patterns are shown in Figs. 4 and 5.

sublattices, $\Delta(t) = (N_A^c(t) - N_B^c(t))/N$, yet gives no information about the spatial distribution of particles within the sublattices. The unusual damped oscillations in the strong quench regime, as shown in Fig. 3, thus could be caused by the onset of spatial inhomogeneity. To examine this scenario, the top panels in Figs. 4 and 5 show the snapshots of on-

site particle number $n_i(t) = \rho_{ii}(t)$ at different times after the quench for the two settings in Figs. 3(a) and 3(b), respectively. As clearly shown in these snapshots, highly complex patterns develop in the postquench states.

Careful examinations show that the quench-induced inhomogeneity mostly is in the form of longer wavelength density modulations on top of the checkerboard CDW order. To better characterize such super modulations of particle density, it is convenient to introduce a scalar order parameter field for the local CDW order

$$\phi(\mathbf{r}_i) = \left(n_i - \frac{1}{4} \sum_j 'n_j \right) \exp(i\mathbf{Q} \cdot \mathbf{r}_i), \quad (24)$$

where the prime in the second term again indicates that the summation is restricted to the nearest neighbors of site i . This local parameter essentially measures the difference of the particle number at a given site and that of its nearest neighbors. A nonzero ϕ_i thus indicates the presence of local particle modulation around site i . The phase factor $\exp(i\mathbf{Q}_i \cdot \mathbf{r}_i) = \pm 1$ is introduced to account for the short-distance checkerboard modulation within a CDW domain. In a perfect checkerboard CDW state, this local order parameter becomes site-independent and is given by the overall CDW order parameter $\Delta(t)$ defined in Eq. (23).

Snapshots of this scalar order parameter ϕ_i corresponding to the particle density profiles at the top row of Figs. 4 and 5 are shown in the respective bottom panels. These results highlight a supermodulation of particle density, as demonstrated by the quasiperiodic square-like patterns in the ϕ_i field, which itself represents a ultrashort-period checkerboard density modulation.

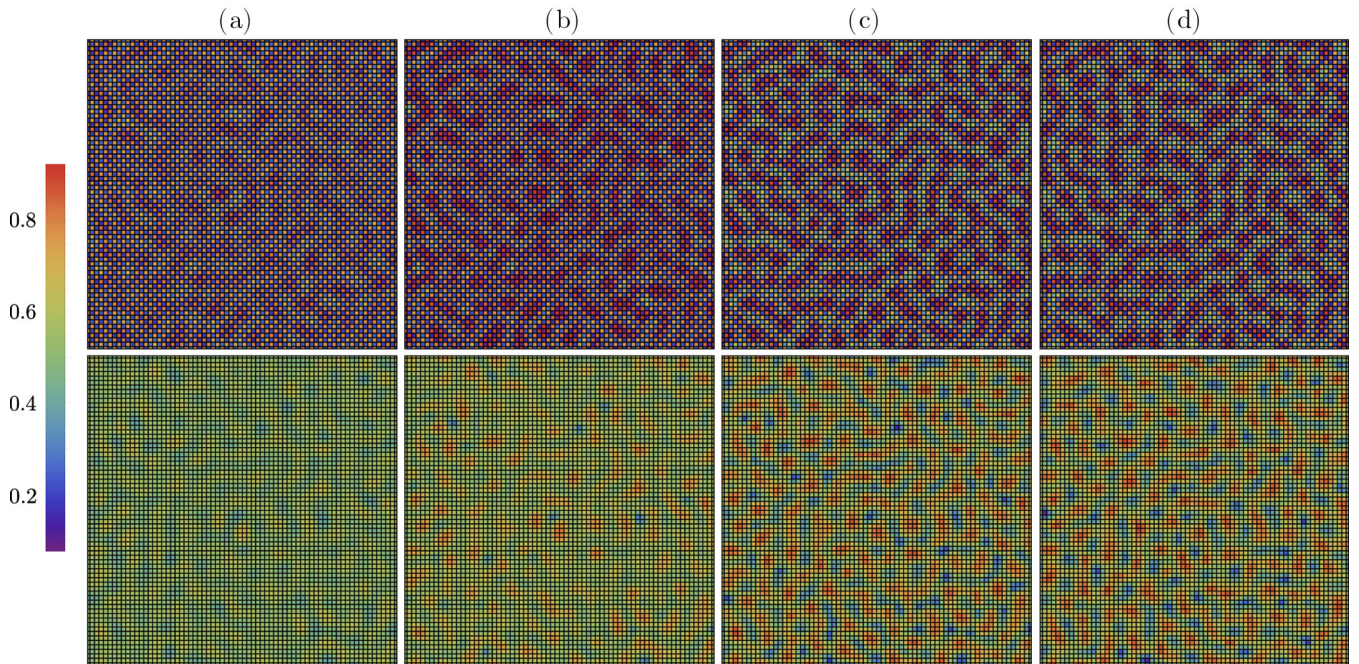


FIG. 4. Snapshots of particle density $n_i = \rho_{ii}$ distributions (top) and local CDW order parameter ϕ_i (bottom) at different time steps after a quantum quench from $V_i = 0.5$ to $V_f = 5.0$. The corresponding checkerboard CDW order as a function of time is shown in Fig. 3(a). Note that the Ising order parameter field, while exhibiting complex patterns, remains positive throughout the relaxation process. (a) $t = 6$, (b) $t = 8$, (c) $t = 10$, and (d) $t = 20$.

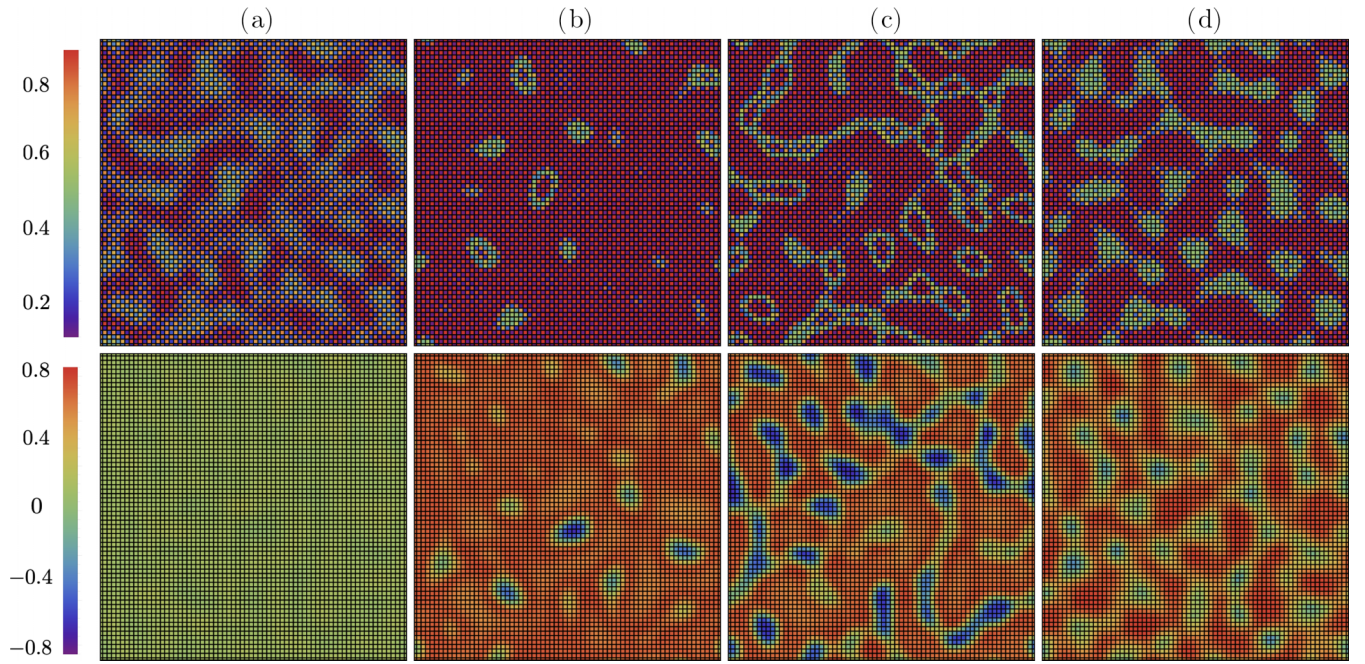


FIG. 5. Snapshots of particle density $n_i = \rho_{ii}$ distributions (top) and local CDW order parameter ϕ_i (bottom) at different time steps after a quantum quench from $V_i = 0.1$ to $V_f = 1.5$. The corresponding checkerboard CDW order as a function of time is shown in Fig. 3(b). The interfaces that separate CDW domains of opposite signs correspond to the finite green lines with a nearly constant fermion density of $\rho_{ii} \sim 0.5$ in the top panels. (a) $t = 6$, (b) $t = 8$, (c) $t = 10$, and (d) $t = 30$.

In the first case where the interaction is quenched from $V_i = 0.5$ to $V_f = 5.0$, the local CDW order parameter ϕ_i remains positive throughout the whole system as shown in Fig. 4. This overall positive ϕ field indicates that a long-range coherence of the initial checkerboard CDW is preserved in the strong quench process. The complex patterns observed in our real-space simulations thus correspond to additional long-wavelength density modulations within a coherent checkerboard domain inherent from the initial CDW state before the quench. This underlying coherent checkerboard order is also consistent with the nearly constant CDW order parameter after the collapse of the oscillations shown in Fig. 3. If we use the discrete Ising variable $\sigma_i = \text{sign } \phi_i$ to characterize such postquench states, they would be very different from configurations observed in thermal quenches from a random state to the low-temperature phase of a broken Z_2 symmetry [93,94]. Due to the locality of thermal relaxations, a temperature quench typically results in multiple Ising domains of *both* signs $\sigma = \pm 1$ that coexist in a heterogeneous state.

On the other hand, for quenches starting from a much smaller V_i as demonstrated in the bottom panels of Fig. 5, Ising domains of opposite signs indeed emerge in the postquench states. In this case, the initial state before the quench exhibits a homogeneous CDW order with a small positive value $\phi \sim 10^{-2}$. Immediately after the quench, the collapse of the coherent oscillation gives rise to a heterogeneous state where multiple CDW domains with $\sigma_i = \text{sign } \phi_i = -1$ are embedded in a background of positive CDW order parameter ϕ ; see Figs. 5(b) and 5(c). The interfaces that separate Ising domains of opposite signs are of a finite width with a nearly constant particle density of $\rho_{ii} \sim 0.5$. As the system further relaxes, those Ising domains with a negative ϕ gradually revert back to

the positive sign, yet with a rather small particle modulation as shown in Fig. 5(d).

To further characterize the emergent density patterns, we compute the corresponding structure factor

$$S(\mathbf{q}, t) = |\tilde{n}(\mathbf{q}, t)|^2, \quad (25)$$

where $\tilde{n}(\mathbf{q}, t)$ is the Fourier transform of the time-dependent particle density $n_i(t) = \rho_{ii}(t)$. In terms of the momentum-space density matrix introduced in Eq. (16), the amplitude of density modulation at wave vector \mathbf{q} is

$$\tilde{n}(\mathbf{q}, t) = \frac{1}{\sqrt{N}} \sum_{\mathbf{k}} \rho_{\mathbf{k}, \mathbf{k}+\mathbf{q}}(t). \quad (26)$$

Figure 6 shows the structure factors of the postquench states at a few selected times after a quench from $V_i = 0.5$ to $V_f = 5$. These figures are obtained by averaging over 90 independent von Neumann dynamics simulations on a $N = 70 \times 70$ system. In the early stage of the postquench relaxation, the coherent oscillation of a spatially homogeneous CDW order gives rise to a delta-function peak in the structure factor shown in Fig. 6(a). As the system further relaxes, the emergence of spatial inhomogeneity corresponds to the gradual growth of a ring-like feature around the delta-peak, as shown in Figs. 6(b)–6(d). The higher intensity points on the ring correspond to the unstable modes that lead to the pattern formation. The ring-like feature is also characteristic of the labyrinthine structures observed in many pattern-forming systems. Labyrinths are spatial structures where local stripe orders with random orientations fail to develop into a long-range order [95,96].

In our case, the super modulations of particle densities shown in Fig. 4 seem to be a combination of local stripe

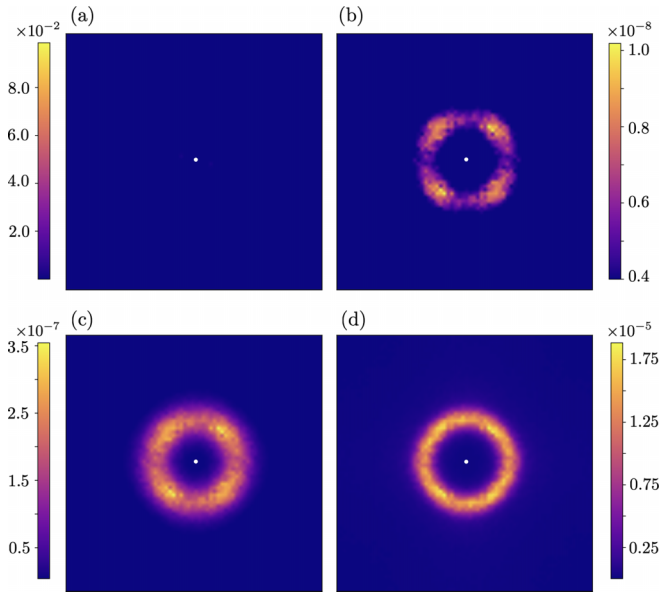


FIG. 6. Structure factors $S(\mathbf{k}, t)$ at various time steps after a quantum quench from $V_i = 0.5$ to $V_f = 5.0$ at time $t = 0$. The simulated system size is $N = 70 \times 70$. The results are obtained by averaging over 90 independent von Neumann dynamics simulations. The white dot at $\mathbf{Q} = (\pi, \pi)$ corresponds to a dominant checkerboard CDW order. The scale of the color bars in panels (b)–(d) is chosen to highlight the emergent unstable modes. (a) $t = 2.5$, (b) $t = 4.0$, (c) $t = 5.0$, and (d) $t = 25$.

and local checkerboard patterns. A domain of local stripe modulation on top of the ultrashort period checkerboard CDW is represented by a pair of wave vectors $\mathbf{Q} \pm \eta \hat{\mathbf{n}}$, where η denotes the modulation wave number and $\hat{\mathbf{n}}$ is a unit vector indicating the orientation of the stripe. Similarly, a domain of checkerboard supermodulation on top of the (π, π) CDW order is characterized by a quadrupole of wave vectors $\mathbf{Q} \pm \eta \hat{\mathbf{n}}_1$ and $\mathbf{Q} \pm \eta \hat{\mathbf{n}}_2$, where $\hat{\mathbf{n}}_1$ and $\hat{\mathbf{n}}_2$ are a pair of orthogonal unit vectors. The inhomogeneous CDW states obtained in our real-space simulations can be viewed as consisting of multiple domains with random unit vectors $\hat{\mathbf{n}}$. The lack of long-range orientational order thus leads to the formation of a ring centered at \mathbf{Q} as shown in Fig. 6(d).

The modulations of the local CDW order parameter can be characterized by two length scales: the modulation period λ of the superstructure (stripes or checkerboard) and the correlation length ξ , or characteristic size of superstructure domains. These two length scales are related to the ring feature in the structure factor $S(\mathbf{q})$ discussed above. The modulation length is given by the inverse of the radius η , while the correlation length is proportional to the inverse of the width of the ring. Specifically, the modulation period can be computed as $\lambda = 2\pi / \langle |\mathbf{q} - \mathbf{Q}| \rangle$, where the angle bracket indicates average using the structure factor $S(\mathbf{q})$ as the weighting factor. A similar formula for the averaged width of the ring can be used to compute the correlation length.

The evolution of these two length scales after a quench from $V_i = 0.5$ to $V_f = 5.0$ is shown in Fig. 7. Two characteristic times t_1 and t_2 are introduced to characterize the initial relaxation of the postquench states. As a homogeneous CDW order is preserved in the initial oscillation period, the

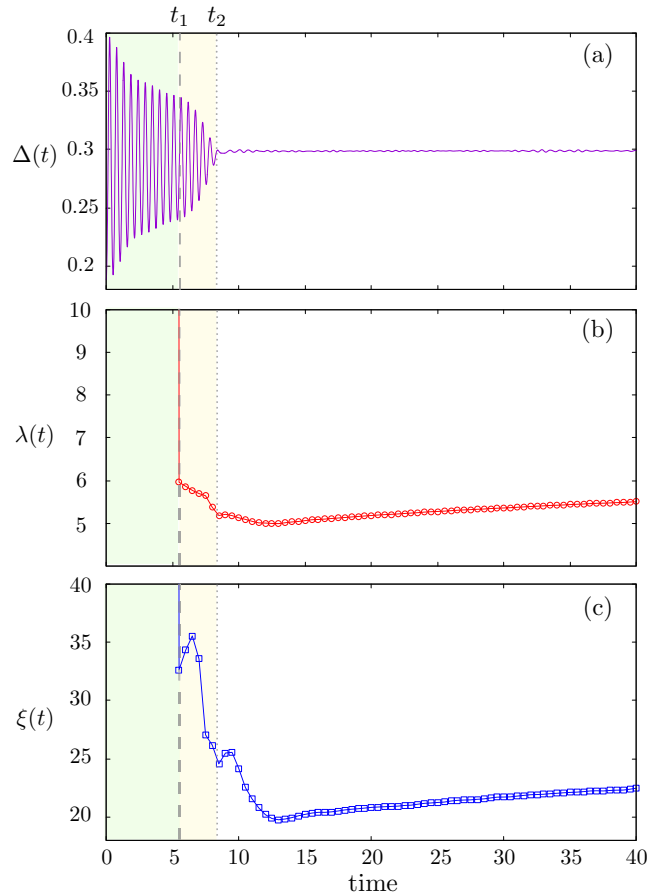


FIG. 7. Postquench dynamics in the regime with emergent pattern formation for a quench from $V_i = 0.5$ to $V_f = 5.0$. (a) Time dependence of the CDW order parameter $\Delta(t)$. (b) Modulation length $\lambda(t)$, and (c) correlation length vs time. The two characteristic times t_1 and t_2 mark the onset of spatial inhomogeneity and the collapse of coherent oscillations, respectively.

correlation length is of the order of the system size and the modulation period is ill defined. The onset of inhomogeneity is signaled by a sudden drop of the correlation length at time t_1 . We also note that the supermodulation patterns corresponding to a finite λ emerges immediately at the onset of inhomogeneity at t_1 . This indicates that the pattern formation here is generated by a quick growth of the unstable modes that becomes significant at t_1 . The emergence of spatial inhomogeneity also accelerates the decline of the oscillation amplitude, and the CDW order Δ settles to a constant at time t_2 , although small fluctuations can still be seen afterward.

We also note that both length scales λ and ξ of the quasi-steady states at late stage of the relaxation depend on the depth V_f/V_i of the interaction quench. This is demonstrated by the snapshots, shown in Figs. 8(a)–8(d), of the late-stage local CDW order parameter ϕ_i for four different final V_f with the same initial interaction $V_i = 0.5$. Long-wavelength supermodulations can be clearly seen in an otherwise overall positive ϕ_i field. As discussed above, this overall positive CDW order indicates that a coherent (π, π) checkerboard density modulation persists in the background for these quench parameters. The modulation period and co-

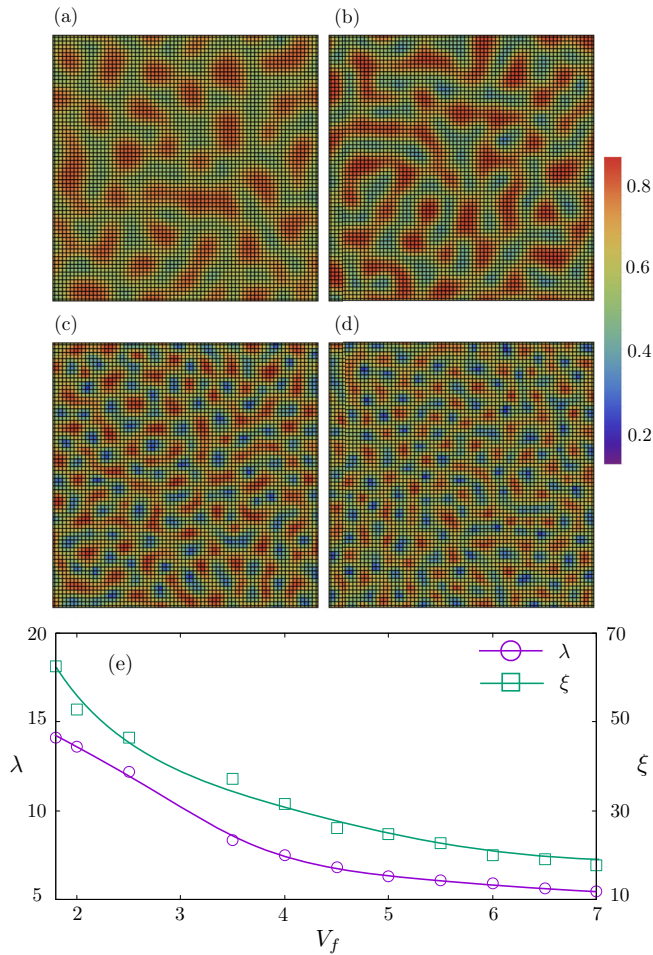


FIG. 8. Local CDW order parameter field at late stage of the quantum quench for (a) $V_f = 2.0$, (b) $V_f = 2.5$, (c) $V_f = 4.0$, and (d) $V_f = 5.0$ with the initial interaction set at $V_i = 0.5$. (e) The modulation length λ , and the correlation length ξ vs V_f with a fixed initial $V_i = 0.5$.

herent length of these superstructures versus the final V_f are shown in Fig. 8(e) at time $t \sim 200$ after the quench. Both length scales decrease with an increasing V_f . Overall, the postquench system exhibits a higher level of inhomogeneity with a stronger quench. The dependence of the modulation period on V_f is related to the instability mechanism for the pattern formation, which will be left in future work. On the other hand, the reduced correlation length ξ in the presence of a stronger quench is likely due to the locality of the pattern formation process in a scenario similar to the Kibble-Zurek mechanism.

VI. CONCLUSIONS AND OUTLOOK

To summarize, we have presented a comprehensive study of quantum quench dynamics of CDW states in the t - V model. For the square-lattice model at half-filling, the checkerboard CDW order can be well described by a self-consistent mean-field theory, which can be generalized to include dynamics via the time-dependent variational principle. This approach essen-

tially describes the evolution of a Slater determinant CDW state and is equivalent to the well-known time-dependent Hartree-Fock (TDHF) theory. Assuming that a homogeneous CDW state is maintained throughout the interaction quench, we show that the TDHF is reduced to an Anderson pseudospin theory, which is widely used for the coherent dynamics of order parameter field in the collisionless limit. Our extensive quench simulations produce three dynamical behaviors of the CDW order, namely, the phase-locked persistent oscillation, Landau-damped oscillation, and dynamical vanishing of the order parameter. These are consistent with previously reported dynamical phases induced by interaction quenches of symmetry-breaking phases.

To incorporate spatial inhomogeneity into the quench dynamics, an efficient nonlinear von Neumann equation is obtained from the real-space TDHF theory to describe the evolution of the postquench CDW state. For strong quenches starting from a relatively small initial interaction, our large-scale real-space simulations uncover complex pattern formation in the postquench CDW states. The onset of spatial inhomogeneity effectively introduces a dephasing mechanism, leading to the collapse of the otherwise phase-locked oscillations of the CDW order parameter. The quench-induced spatial patterns are characterized by domains of super modulations of the particle density in the form of stripes or checkerboards on top of the original ultrashort-period CDW order. However, the lack of orientational coherence between different domains leads to overall disordered patterns similar to the labyrinthine structures observed in many pattern-forming systems. The resultant structure factor is characterized by a ring-like feature centered at the checkerboard wave vector $\mathbf{Q} = (\pi, \pi)$. The inverse radius and width of the ring correspond to the super modulation period and coherent length, respectively, of the inhomogeneous CDW state.

The emergence of the super modulation patterns on top of the CDW order is caused by unstable modes with wave vectors $\mathbf{q} = \mathbf{Q} + (2\pi/\lambda)\hat{\mathbf{n}}$, where λ is the modulation period. A common mechanism for pattern formation is the parametric instability where a pair of unstable modes grow spontaneously from the decay of an initial driver mode through nonlinear interactions. Indeed, the parametric instability has been shown to result in the decay of a uniform oscillating pairing order parameter and the emergence of an inhomogeneous Cooper-pair turbulence state. A possible scenario for pattern formation of the quenched t - V model is the decay of the checkerboard CDW order parameter into a pair of such unstable modes \mathbf{q}_1 and \mathbf{q}_2 through the parametric instability mechanism. However, for general modulation period λ , the momentum is not conserved in this process $\mathbf{q}_1 + \mathbf{q}_2 \neq \mathbf{Q}$. This consideration thus rules out the instability as the direct decay of the phase-locked oscillation of the CDW order. On the other hand, detailed examinations of the initial relaxation after a quench show that the unstable modes indeed appear in pairs, suggesting a modified version of the parametric instability. A detailed study of the instability mechanism will be presented elsewhere.

As discussed above, similar interaction quenches of the 1D spinless t - V model, which is equivalent to a spin-1/2 XXZ system, have been studied using the iTEBD method

[82,83]. The system is initially prepared in a state of classical Néel order, corresponding to a product CDW state $|0\rangle \otimes |1\rangle \otimes |0\rangle \otimes |1\rangle \otimes \dots$, where $|0\rangle$ and $|1\rangle$ denote empty and occupied sites, respectively. It is then subjected to the unitary evolution of the t - V model with a finite V . Since 1D Ising order cannot survive in such short-range models at any finite temperatures, the initial CDW order is destroyed by the energy density deposited by the quantum quench. On the other hand, as long-range Ising order is stable at low enough temperatures in 2D, the postquench state of the t - V model can relax to a stable CDW state for sufficiently small energy injection from the quench.

Our paper underscores the importance of dynamical inhomogeneity in quantum quench dynamics of many-body systems. Indeed, here we demonstrate that the postquench dynamics of a many-fermion system with a simple broken Z_2 symmetry is susceptible to pattern-formation instability, even in the collisionless limit. The emergence of complex patterns in this limit is entirely due to the nonlinear dynamics of order parameter fields. Our results indicate that pattern formation is likely to be a generic feature of quantum quenches with more complex order parameters. It is worth

noting that while pattern formation in classical physics is a well-studied subject, quench-induced spatial inhomogeneity in quantum many-body systems is a relatively unexplored area of research. In addition to the nonlinearity originating from the many-body interactions, the quantum fermionic statistics could play a crucial role in the instability mechanisms. For symmetry-breaking phases characterized by complex ordering structures, the associated pattern formation and mechanisms might be closely related to the topological defects of the corresponding order parameter fields. Finally, inclusion of incoherent processes, such as quantum fluctuations, quasi-particle scattering, and energy dissipation, are expected to produce even richer spatiotemporal dynamical behaviors of the postquench states.

ACKNOWLEDGMENTS

The work was supported by the U.S. Department of Energy, Basic Energy Sciences under Contract No. DE-SC0020330. L.Y. acknowledges the support of Jefferson Fellowship. The authors also acknowledge the support of Research Computing at the University of Virginia.

-
- [1] J. Eisert, M. Friesdorf, and C. Gogolin, Quantum many-body systems out of equilibrium, *Nat. Phys.* **11**, 124 (2015).
- [2] A. Mitra, Quantum quench dynamics, *Annu. Rev. Condens. Matter Phys.* **9**, 245 (2018).
- [3] A. Polkovnikov, K. Sengupta, A. Silva, and M. Vengalattore, Colloquium: Nonequilibrium dynamics of closed interacting quantum systems, *Rev. Mod. Phys.* **83**, 863 (2011).
- [4] I. Bloch, J. Dalibard, and W. Zwerger, Many-body physics with ultracold gases, *Rev. Mod. Phys.* **80**, 885 (2008).
- [5] M. A. Cazalilla, R. Citro, T. Giamarchi, E. Orignac, and M. Rigol, One dimensional bosons: From condensed matter systems to ultracold gases, *Rev. Mod. Phys.* **83**, 1405 (2011).
- [6] D. Fausti, R. Tobey, N. Dean, S. Kaiser, A. Dienst, M. C. Hoffmann, S. Pyon, T. Takayama, H. Takagi, and A. Cavalleri, Light-induced superconductivity in a stripe-ordered cuprate, *Science* **331**, 189 (2011).
- [7] R. Matsunaga and R. Shimano, Nonequilibrium BCS state dynamics induced by intense terahertz pulses in a superconducting NbN film, *Phys. Rev. Lett.* **109**, 187002 (2012).
- [8] R. Matsunaga, Y. I. Hamada, K. Makise, Y. Uzawa, H. Terai, Z. Wang, and R. Shimano, Higgs amplitude mode in the BCS superconductors $\text{Nb}_{1-x}\text{Ti}_x\text{N}$ induced by terahertz pulse excitation, *Phys. Rev. Lett.* **111**, 057002 (2013).
- [9] B. Mansart, J. Lorenzana, A. Mann, A. Odeh, M. Scarongella, M. Chergui, and F. Carbone, Coupling of a high-energy excitation to superconducting quasiparticles in a cuprate from coherent charge fluctuation spectroscopy, *Proc. Natl. Acad. Sci. USA* **110**, 4539 (2013).
- [10] R. Matsunaga, N. Tsuji, H. Fujita, A. Sugioka, K. Makise, Y. Uzawa, H. Terai, Z. Wang, H. Aoki, and R. Shimano, Light-induced collective pseudospin precession resonating with Higgs mode in a superconductor, *Science* **345**, 1145 (2014).
- [11] M. Mitrano, A. Cantaluppi, D. Nicoletti, S. Kaiser, A. Perucchi, S. Lupi, P. Di Pietro, D. Pontiroli, M. Riccò, S. R. Clark *et al.*, Possible light-induced superconductivity in $\text{K}_3\text{C}_6\text{O}$ at high temperature, *Nature (London)* **530**, 461 (2016).
- [12] C. Kollath, A. M. Läuchli, and E. Altman, Quench dynamics and nonequilibrium phase diagram of the Bose-Hubbard model, *Phys. Rev. Lett.* **98**, 180601 (2007).
- [13] J. Berges, A. Rothkopf, and J. Schmidt, Nonthermal fixed points: Effective weak coupling for strongly correlated systems far from equilibrium, *Phys. Rev. Lett.* **101**, 041603 (2008).
- [14] M. Cramer, C. M. Dawson, J. Eisert, and T. J. Osborne, Exact relaxation in a class of nonequilibrium quantum lattice systems, *Phys. Rev. Lett.* **100**, 030602 (2008).
- [15] A. Flesch, M. Cramer, I. P. McCulloch, U. Schollwöck, and J. Eisert, Probing local relaxation of cold atoms in optical superlattices, *Phys. Rev. A* **78**, 033608 (2008).
- [16] M. Rigol, Breakdown of thermalization in finite one-dimensional systems, *Phys. Rev. Lett.* **103**, 100403 (2009).
- [17] J. Dziarmaga, Dynamics of a quantum phase transition and relaxation to a steady state, *Adv. Phys.* **59**, 1063 (2010).
- [18] C. Gogolin, M. P. Müller, and J. Eisert, Absence of thermalization in nonintegrable systems, *Phys. Rev. Lett.* **106**, 040401 (2011).
- [19] S. Erne, R. Bücker, T. Gasenzer, J. Berges, and J. Schmiedmayer, Universal dynamics in an isolated one-dimensional Bose gas far from equilibrium, *Nature (London)* **563**, 225 (2018).
- [20] T. Kinoshita, T. Wenger, and D. S. Weiss, A quantum Newton's cradle, *Nature (London)* **440**, 900 (2006).
- [21] S. Trotzky, Y.-A. Chen, A. Flesch, I. P. McCulloch, U. Schollwöck, J. Eisert, and I. Bloch, Probing the relaxation towards equilibrium in an isolated strongly correlated one-dimensional Bose gas, *Nat. Phys.* **8**, 325 (2012).
- [22] M. Schreiber, S. S. Hodgman, P. Bordia, H. P. Lüschen, M. H. Fischer, R. Vosk, E. Altman, U. Schneider, and I. Bloch, Ob-

- ervation of many-body localization of interacting fermions in a quasirandom optical lattice, *Science* **349**, 842 (2015).
- [23] K. Mallayya and M. Rigol, Quantum quenches and relaxation dynamics in the thermodynamic limit, *Phys. Rev. Lett.* **120**, 070603 (2018).
- [24] M. Rigol, Fundamental asymmetry in quenches between integrable and nonintegrable systems, *Phys. Rev. Lett.* **116**, 100601 (2016).
- [25] R. Barnett, A. Polkovnikov, and M. Vengalattore, Prethermalization in quenched spinor condensates, *Phys. Rev. A* **84**, 023606 (2011).
- [26] M. Gring, M. Kuhnert, T. Langen, T. Kitagawa, B. Rauer, M. Schreitl, I. Mazets, D. A. Smith, E. Demler, and J. Schmiedmayer, Relaxation and prethermalization in an isolated quantum system, *Science* **337**, 1318 (2012).
- [27] T. Langen, R. Geiger, M. Kuhnert, B. Rauer, and J. Schmiedmayer, Local emergence of thermal correlations in an isolated quantum many-body system, *Nat. Phys.* **9**, 640 (2013).
- [28] M. Marcuzzi, J. Marino, A. Gambassi, and A. Silva, Prethermalization in a nonintegrable quantum spin chain after a quench, *Phys. Rev. Lett.* **111**, 197203 (2013).
- [29] A. Mitra, Correlation functions in the prethermalized regime after a quantum quench of a spin chain, *Phys. Rev. B* **87**, 205109 (2013).
- [30] N. Nessi, A. Iucci, and M. A. Cazalilla, Quantum quench and prethermalization dynamics in a two-dimensional Fermi gas with long-range interactions, *Phys. Rev. Lett.* **113**, 210402 (2014).
- [31] T. Langen, S. Erne, R. Geiger, B. Rauer, T. Schweigler, M. Kuhnert, W. Rohringer, I. E. Mazets, T. Gasenzer, and J. Schmiedmayer, Experimental observation of a generalized Gibbs ensemble, *Science* **348**, 207 (2015).
- [32] M. Babadi, E. Demler, and M. Knap, Far-from-equilibrium field theory of many-body quantum spin systems: Prethermalization and relaxation of spin spiral states in three dimensions, *Phys. Rev. X* **5**, 041005 (2015).
- [33] B. Bertini, F. H. L. Essler, S. Groha, and N. J. Robinson, Prethermalization and thermalization in models with weak integrability breaking, *Phys. Rev. Lett.* **115**, 180601 (2015).
- [34] T. Langen, T. Gasenzer, and J. Schmiedmayer, Prethermalization and universal dynamics in near-integrable quantum systems, *J. Stat. Mech.* (2016) 064009.
- [35] M. Buchhold, M. Heyl, and S. Diehl, Prethermalization and thermalization of a quenched interacting Luttinger liquid, *Phys. Rev. A* **94**, 013601 (2016).
- [36] J. Marino, M. Eckstein, M. S. Foster, and A. M. Rey, Dynamical phase transitions in the collisionless pre-thermal states of isolated quantum systems: Theory and experiments, *Rep. Prog. Phys.* **85**, 116001 (2022).
- [37] M. Heyl, Dynamical quantum phase transitions in systems with broken-symmetry phases, *Phys. Rev. Lett.* **113**, 205701 (2014).
- [38] R. A. Barankov, L. S. Levitov, and B. Z. Spivak, Collective rabi oscillations and solitons in a time-dependent BCS pairing problem, *Phys. Rev. Lett.* **93**, 160401 (2004).
- [39] R. A. Barankov and L. S. Levitov, Synchronization in the BCS pairing dynamics as a critical phenomenon, *Phys. Rev. Lett.* **96**, 230403 (2006).
- [40] E. A. Yuzbashyan, O. Tsypliyatyev, and B. L. Altshuler, Relaxation and persistent oscillations of the order parameter in fermionic condensates, *Phys. Rev. Lett.* **96**, 097005 (2006).
- [41] E. A. Yuzbashyan and M. Dzero, Dynamical vanishing of the order parameter in a fermionic condensate, *Phys. Rev. Lett.* **96**, 230404 (2006).
- [42] V. Gurarie, Nonequilibrium dynamics of weakly and strongly paired superconductors, *Phys. Rev. Lett.* **103**, 075301 (2009).
- [43] M. S. Foster, M. Dzero, V. Gurarie, and E. A. Yuzbashyan, Quantum quench in a $p + ip$ superfluid: Winding numbers and topological states far from equilibrium, *Phys. Rev. B* **88**, 104511 (2013).
- [44] M. S. Foster, V. Gurarie, M. Dzero, and E. A. Yuzbashyan, Quench-induced Floquet topological p -wave superfluids, *Phys. Rev. Lett.* **113**, 076403 (2014).
- [45] N. Tsuji, M. Eckstein, and P. Werner, Nonthermal antiferromagnetic order and nonequilibrium criticality in the Hubbard model, *Phys. Rev. Lett.* **110**, 136404 (2013).
- [46] Y. Dong, L. Dong, M. Gong, and H. Pu, Dynamical phases in quenched spin-orbit-coupled degenerate Fermi gas, *Nat. Commun.* **6**, 6103 (2015).
- [47] F. Peronaci, M. Schiró, and M. Capone, Transient dynamics of d -wave superconductors after a sudden excitation, *Phys. Rev. Lett.* **115**, 257001 (2015).
- [48] B. Dóra, M. Haque, F. Pollmann, and B. Hetényi, Quantum quench in two dimensions using the variational Baeriswyl wave function, *Phys. Rev. B* **93**, 115124 (2016).
- [49] I. V. Blinov, P. Ribeiro, and A. N. Rubtsov, Post-quench dynamics and suppression of thermalization in an open half-filled Hubbard layer, *Phys. Rev. B* **95**, 024309 (2017).
- [50] Y.-Z. Chou, Y. Liao, and M. S. Foster, Twisting anderson pseudospins with light: Quench dynamics in terahertz-pumped BCS superconductors, *Phys. Rev. B* **95**, 104507 (2017).
- [51] S. Yoon and G. Watanabe, Pairing dynamics of polar states in a quenched p -wave superfluid Fermi gas, *Phys. Rev. Lett.* **119**, 100401 (2017).
- [52] S. Hannibal, P. Kettmann, M. D. Croitoru, V. M. Axt, and T. Kuhn, Dynamical vanishing of the order parameter in a confined Bardeen-Cooper-Schrieffer Fermi gas after an interaction quench, *Phys. Rev. A* **97**, 013619 (2018).
- [53] S. Hannibal, P. Kettmann, M. D. Croitoru, V. M. Axt, and T. Kuhn, Persistent oscillations of the order parameter and interaction quench phase diagram for a confined Bardeen-Cooper-Schrieffer Fermi gas, *Phys. Rev. A* **98**, 053605 (2018).
- [54] T. Cui, M. Schütt, P. P. Orth, and R. M. Fernandes, Postquench gap dynamics of two-band superconductors, *Phys. Rev. B* **100**, 144513 (2019).
- [55] J. A. Scaramazza, P. Smacchia, and E. A. Yuzbashyan, Consequences of integrability breaking in quench dynamics of pairing Hamiltonians, *Phys. Rev. B* **99**, 054520 (2019).
- [56] Y. Chen and Z. Cai, Persistent oscillations versus thermalization in the quench dynamics of quantum gases with long-range interactions, *Phys. Rev. A* **101**, 023611 (2020).
- [57] P. W. Anderson, Random-phase approximation in the theory of superconductivity, *Phys. Rev.* **112**, 1900 (1958).
- [58] T. W. B. Kibble, Topology of cosmic domains and strings, *J. Phys. A: Math. Gen.* **9**, 1387 (1976).
- [59] W. H. Zurek, Cosmological experiments in superfluid helium? *Nature (London)* **317**, 505 (1985).

- [60] B. Damski, The simplest quantum model supporting the Kibble-Zurek mechanism of topological defect production: Landau-Zener transitions from a new perspective, *Phys. Rev. Lett.* **95**, 035701 (2005).
- [61] K. Sengupta, D. Sen, and S. Mondal, Exact results for quench dynamics and defect production in a two-dimensional model, *Phys. Rev. Lett.* **100**, 077204 (2008).
- [62] W. H. Zurek, U. Dorner, and P. Zoller, Dynamics of a quantum phase transition, *Phys. Rev. Lett.* **95**, 105701 (2005).
- [63] L. Mathey and A. Polkovnikov, Light cone dynamics and reverse Kibble-Zurek mechanism in two-dimensional superfluids following a quantum quench, *Phys. Rev. A* **81**, 033605 (2010).
- [64] A. Chandran, A. Erez, S. S. Gubser, and S. L. Sondhi, Kibble-Zurek problem: Universality and the scaling limit, *Phys. Rev. B* **86**, 064304 (2012).
- [65] A. del Campo, Universal statistics of topological defects formed in a quantum phase transition, *Phys. Rev. Lett.* **121**, 200601 (2018).
- [66] M. Dzero, E. A. Yuzbashyan, and B. L. Altshuler, Cooper pair turbulence in atomic Fermi gases, *Europhys. Lett.* **85**, 20004 (2009).
- [67] G.-W. Chern and K. Barros, Nonequilibrium dynamics of superconductivity in the attractive Hubbard model, *Phys. Rev. B* **99**, 035162 (2019).
- [68] B. Huang, X. Yang, N. Xu, J. Zhou, and M. Gong, Dynamical instability with respect to finite-momentum pairing in quenched BCS superconducting phases, *Phys. Rev. B* **99**, 014517 (2019).
- [69] M. Eckstein, M. Kollar, and P. Werner, Thermalization after an interaction quench in the Hubbard model, *Phys. Rev. Lett.* **103**, 056403 (2009).
- [70] M. Schiró and M. Fabrizio, Time-dependent mean field theory for quench dynamics in correlated electron systems, *Phys. Rev. Lett.* **105**, 076401 (2010).
- [71] G.-W. Chern, Dynamic inhomogeneities and phase separation after quantum quenches in strongly correlated systems, [arXiv:1711.07972](https://arxiv.org/abs/1711.07972).
- [72] G. Nicolis and I. Prigogine, *Self Organization in Non Equilibrium Systems* (Wiley, New York, 1977).
- [73] M. C. Cross and P. C. Hohenberg, Pattern formation outside of equilibrium, *Rev. Mod. Phys.* **65**, 851 (1993).
- [74] A. J. Koch and H. Meinhardt, Biological pattern formation: From basic mechanisms to complex structures, *Rev. Mod. Phys.* **66**, 1481 (1994).
- [75] L. Pismen, *Patterns and Interfaces in Dissipative Dynamics* (Springer, New York, 2006).
- [76] M. Cross and H. Greenside, *Pattern Formation and Dynamics in Non-Equilibrium Systems* (Cambridge University Press, Cambridge, 2009).
- [77] J. H. Robertson, R. Senese, and F. H. L. Essler, Decay of long-lived oscillations after quantum quenches in gapped interacting quantum systems, *Phys. Rev. A* **109**, 032208 (2024).
- [78] S. R. White, Density matrix formulation for quantum renormalization groups, *Phys. Rev. Lett.* **69**, 2863 (1992).
- [79] U. Schollwöck, The density-matrix renormalization group, *Rev. Mod. Phys.* **77**, 259 (2005).
- [80] G. Vidal, Efficient classical simulation of slightly entangled quantum computations, *Phys. Rev. Lett.* **91**, 147902 (2003).
- [81] S. R. White and A. E. Feiguin, Real-time evolution using the density matrix renormalization group, *Phys. Rev. Lett.* **93**, 076401 (2004).
- [82] M. Fagotti, M. Collura, F. H. L. Essler, and P. Calabrese, Relaxation after quantum quenches in the spin- $\frac{1}{2}$ Heisenberg XXZ chain, *Phys. Rev. B* **89**, 125101 (2014).
- [83] M. Collura and F. H. L. Essler, How order melts after quantum quenches, *Phys. Rev. B* **101**, 041110(R) (2020).
- [84] P. Ring and P. Schuck, *The Nuclear Many-Body Problem* (Springer-Verlag, Berlin, 1980).
- [85] A. D. McLachlan and M. A. Ball, Time-dependent Hartree-Fock theory for molecules, *Rev. Mod. Phys.* **36**, 844 (1964).
- [86] E. Deumens, A. Diz, R. Longo, and Y. Öhrn, Time-dependent theoretical treatments of the dynamics of electrons and nuclei in molecular systems, *Rev. Mod. Phys.* **66**, 917 (1994).
- [87] P. A. M. Dirac, Note on exchange phenomena in the thomas atom, *Math. Proc. Cambridge Philos. Soc.* **26**, 376 (1930).
- [88] J. Frenkel, *Wave Mechanics: Advanced General Theory* (Oxford University Press, Oxford, 1934).
- [89] J. Haegeman, J. I. Cirac, T. J. Osborne, I. Pižorn, H. Verschelde, and F. Verstraete, Time-dependent variational principle for quantum lattices, *Phys. Rev. Lett.* **107**, 070601 (2011).
- [90] J. Haegeman, C. Lubich, I. Oseledets, B. Vandereycken, and F. Verstraete, Unifying time evolution and optimization with matrix product states, *Phys. Rev. B* **94**, 165116 (2016).
- [91] F. Bloch, Nuclear induction, *Phys. Rev.* **70**, 460 (1946).
- [92] A. F. Volkov and S. M. Kogan, Collisionless relaxation of the energy gap in superconductors, *Sov. Phys.-JETP* **38**, 1018 (1974).
- [93] A. J. Bray, Theory of phase-ordering kinetics, *Adv. Phys.* **43**, 357 (1994).
- [94] S. Puri and V. Wadhawan, *Kinetics of Phase Transitions* (CRC Press, Boca Raton, FL, 2009).
- [95] A. C. Newell and Y. Pomeau, Turbulent crystals in macroscopic systems, *J. Phys. A: Math. Gen.* **26**, L429 (1993).
- [96] M. Le Berre, E. Ressayre, A. Tallet, Y. Pomeau, and L. Di Menza, Example of a chaotic crystal: The labyrinth, *Phys. Rev. E* **66**, 026203 (2002).